Fine Chemical Engineering
https://ojs.wiserpub.com/index.php/FCE/

Research Article

A Simple and Scalable One-Pot Chemical Reduction and Functionalization of Reduced Graphene Oxide Films for Flexible Supercapacitor Applications

Hamdane Akbi[1*], Souleymen Rafai[1], Ahmed Mekki[1], Sabri Touidjine[2], Ahmed Saim[1]

[1]Teaching and Research Unit in Materials Physicochemistry, Military Polytechnic School (EMP), BP 17, Bordj El Bahri, Algiers, 16046, Algeria
[2]Teaching and Research Unit in Energy Processes, Military Polytechnic School (EMP), BP 17, Bordj El Bahri, Algiers, 16046, Algeria
E-mail: D_AKBI.HAMDANE@emp.dz

Received: 1 June 2025; **Revised:** 31 August 2025; **Accepted:** 31 October 2025

Graphical Abstract:

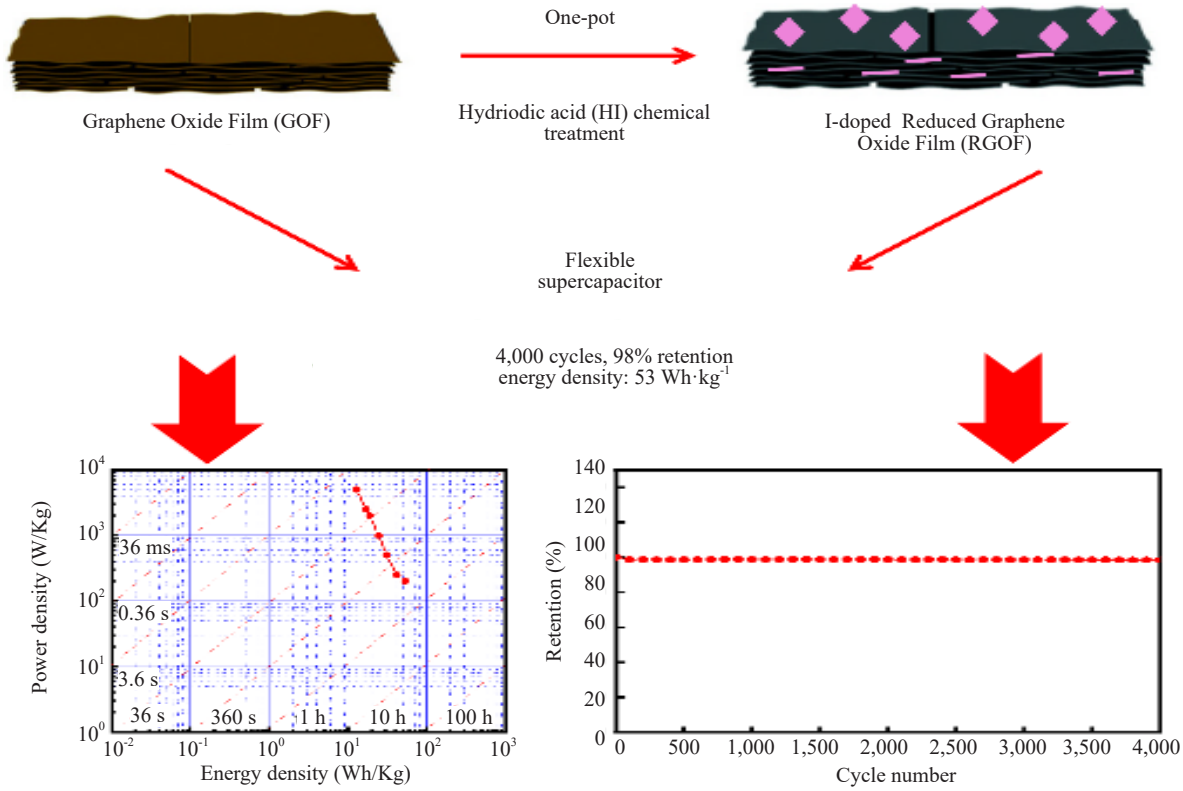

DOI: https://doi.org/10.37256/fce.7120267340

Abstract: This study presents a one-pot, low-cost, and scalable method for preparing chemically Reduced Graphene Oxide Films (RGOFs) doped with iodine groups for supercapacitor applications. The Graphene Oxide Film (GOF) was first fabricated via a simple solution-casting technique, followed by chemical reduction using Hydriodic acid (HI) as the reducing agent. The as-prepared GOF and RGOF were thoroughly characterized in terms of their electrical, mechanical, morphological, and structural properties using appropriate analytical techniques. Results indicate that GOF was successfully reduced and functionalized with iodine groups. When tested as supercapacitor electrodes, the films demonstrated nearly ideal capacitive characteristics, delivering a high specific capacitance of ~ 380 $F \cdot g^{-1}$. Furthermore, they maintained good cyclic stability, preserving nearly 98% of their initial capacitance after 4,000 charge/discharge cycles. These promising results highlight the potential of these films as cost-effective and scalable candidates for next-generation high-performance flexible supercapacitors.

***Keywords*:** Hydriodic acid (HI) chemical reduction, Reduced Graphene Oxide Films (RGOF), supercapacitor, electrochemical performance

1. Introduction

The rapid advancement of Portable and Foldable Electronic Devices (PFEDs) has increased the demand for flexible materials that can be used in various components, including energy storage systems. Among these, Flexible Supercapacitors (FSCs) have attracted significant attention due to their appealing characteristics.[1,2] Notably, compared to conventional capacitors, FSCs offer energy densities that are several orders of magnitude higher. Furthermore, they possess higher power densities than most batteries, although their specific energy density is somewhat lower.[3] As a result, extensive research has focused on developing innovative materials with excellent physicochemical properties for FSC applications.[4]

In supercapacitors, the energy density is directly dependent on the specific capacitance and the square of the voltage window. Therefore, enhancing either of these parameters is an effective strategy for increasing energy density. Specific capacitance can be improved by developing novel materials that offer higher specific surface areas and better electrical conductivity compared to existing materials. Additionally, the use of aqueous electrolytes can further enhance specific capacitance due to their smaller ion sizes, which enable more efficient utilization of the electrode surface area.[5] However, the operating voltage window of aqueous electrolytes is theoretically limited to 1.23 V, and practically to about 1.4 V due to kinetic constraints. In contrast, ionic liquids and organic electrolytes offer a promising alternative, as they allow for a significantly wider operating voltage window.[6]

Among the materials that have recently attracted attention for supercapacitor applications, graphene stands out due to its unique mechanical features, excellent electrical conductivity, large specific surface area, and remarkable chemical stability.[7-9] However, pristine graphene is both difficult and expensive to produce.[10] Therefore, significant efforts have been directed toward a more cost-effective alternative. Notably, Reduced Graphene Oxide (RGO) shares many of the desirable physicochemical characteristics of pristine graphene. RGO can be synthesized through the oxidation and exfoliation of abundant graphite, followed by subsequent reduction.[11]

Notably, the oxidation and exfoliation process yields Graphene Oxide (GO), a material characterized by excellent dispersibility in solvents like water, attributed to the introduction of Oxygen-Containing Functional Groups (OCFGs) that render GO hydrophilic.[12] This property facilitates the easy fabrication of free-standing Graphene Oxide Films (GOFs) and coatings on various substrates.[13-16] The graphitic properties of GO-Based Materials (GBMs) can be restored through reduction techniques, which include both thermal and chemical methods.[17] Thermal reduction methods, such as microwave irradiation,[18] heat treatment,[19] and laser scribing,[20] can be employed without damaging the structure of GBMs. However, in the case of GOFs and coatings, chemical reduction using certain reagents may compromise the structural integrity of the GBMs or even damage the underlying substrates.[11]

Due to its freestanding structure, GOF presents significant potential for applications in purification[21] and coating[13] fields. Moreover, its conversion into Reduced GOF (RGOF), along with further functionalization, enhances its suitability for various components in PFEDs, including batteries,[22] displays, flexible thermoelectric generators,[17] and supercapacitors.[23]

Hydroiodic acid (HI) has demonstrated exceptional effectiveness as a reducing agent for GOFs, owing not only to its ability to yield freestanding Reduced Graphene Oxide Films (RGOFs) with superior electrical and mechanical properties, but also to its role in introducing iodine-containing functional groups into the RGOF structure.[24,25] This chemical modification significantly alters the material's physicochemical characteristics, further boosting its suitability for diverse applications, including supercapacitors.[16]

Herein, we introduce a straightforward, rapid, cost-effective, and scalable strategy for fabricating RGOFs through the chemical reduction of GOFs produced via a solution-casting technique. HI served as an efficient reducing agent, enabling the formation of high-quality freestanding RGOFs. The mechanical and electrical properties of the films were thoroughly characterized before and after reduction, accompanied by an in-depth analysis of the structural and morphological transformations induced during the process. Additionally, the electrochemical behavior of the resulting RGOFs was assessed in FSC applications, where they exhibited outstanding performance and long-term stability, underscoring their strong potential for next-generation energy storage technologies. The originality of this work lies in the simultaneous chemical reduction and in situ functionalization achieved through a scalable, one-pot synthesis strategy. This integrated approach not only simplifies fabrication but also enables the production of RGOF-based electrodes with outstanding electrochemical performance, offering a cost-effective pathway toward practical energy storage applications.

2. Experimental

2.1 *Materials and methods*

Graphite oxide was synthesized from graphite microscale powder using the widely adopted modified Hummers method.[26,27] Exfoliation into GO was accomplished by ultrasonically treating the dispersion in a bath sonicator (KQ-500 DB, 250 W). GOF were then produced by solution casting GO dispersions (4.5 mg·mL^{-1}) into a glass mold.

To prepare a GOF with a thickness of 130 μm using the mold mentioned above, the required amount of dispersed GO for casting can be calculated as follows:

$$Q_{GO} = (10\ cm \times 20\ cm) \times (0.81\ mg \cdot cm^{-2})/(4.5\ mg \cdot mL^{-1}).$$

$$Q_{GO} = 36\ mL.$$

Knowing that: 1 cm^2 of GO (130 μm thickness) weighs 0.81 mg and the concentration of the as-prepared GO is 4.5 mg per mL, the Glass mold dimensions are 20 cm ×10 cm.

The resulting films were first air-dried for 48 hours at room temperature, followed by thermal drying at 50 °C for 24 hours. The reduction of GOFs was carried out by immersing GOFs into hydriodic acid (30%) at 70 °C for 45 min. For more details about the fabrication procedures, see our recently published articles.[2,14,17]

2.2 *Characterization*

• **The crystallographic structure** of the materials was analyzed using powder X-Ray Diffraction (XRD) with a Rigaku TTR-III system equipped with Cu Kα radiation (λ = 0.15406 nm).

• **Raman spectroscopy** was performed using a Thermo Scientific DXR spectrometer (532 nm wavelength, 3.0 mW power) in absorbance mode over the range of 100-3,500 cm^{-1} to investigate the vibrational modes of the RGOFs.

• **The microstructure** of the samples was examined using scanning electron microscopy (SEM, JEOL JSM-6480A).

• **Electrical conductivity measurements** of the RGOFs were conducted using the four-point probe technique with a JANDEL RM3000 system. For each RGOF, three measurements were taken to ensure accuracy. The electrical conductivity (σ, S·cm^{-1}) was calculated using the equation $\sigma = 1 / (R \cdot e)$, where e (in cm) represents the RGOF thickness. Three separate electrical conductivity measurements were taken for each film.

• **Tensile strength** tests were carried out using an INSTRON 4505 mechanical testing machine. The thickness of

both GOF and RGOF was measured by SEM. To ensure reproducibility, the tensile strength test was performed three times.

2.3 *Preparation of electrodes and electrochemical measurement*

Concerning the evaluation of the electrochemical performance of RGOFs as an electrode for a supercapacitor, the working electrodes were fabricated by directly pressing the RGOF onto nickel foam, which acted both as a current collector and mechanical support. This configuration ensures good electrical contact while minimizing damage or delamination of the RGOF during measurements. All electrochemical tests were conducted in a standard three-electrode setup, where the Ni foam/RGOF system served as the working electrode, a platinum foil was used as the counter electrode, and a Saturated Calomel Electrode (SCE) functioned as the reference. The electrolyte was a 6 M KOH aqueous solution, chosen for its high ionic conductivity and widespread use in supercapacitor testing. All measurements were carried out at room temperature under ambient conditions. Cyclic Voltammetry (CV), Galvanostatic Charge-Discharge (GCD), and Electrochemical Impedance Spectroscopy (EIS) were performed using a CHI 660C electrochemical workstation. CV curves were recorded over a potential window of -1 to 0 V at various scan rates to evaluate the capacitive behavior. GCD tests were conducted within the same voltage range at different current densities to determine the specific capacitance and rate capability of the electrodes. EIS measurements were carried out at open circuit potential in the frequency range of 100 kHz to 0.005 Hz, using an Alternating Current (AC) perturbation of 5 mV.

3. Results and discussion

3.1 *Sample preparation*

Graphite consists of numerous graphene layers stacked in a well-ordered structure, held together by weak van der Waals interactions.[28] When subjected to strong oxidizing agents, typically in the presence of concentrated acids and oxidants, microscale graphite undergoes chemical oxidation, leading to the incorporation of OCFGs, such as hydroxyl, epoxy, carbonyl, and carboxyl, on both the basal planes and edges of the graphene layers. These functional groups disrupt the π-π stacking between layers, increase the interlayer spacing, and significantly weaken the intersheet interactions.[29] As a result, the oxidized graphite can be readily exfoliated into few-layer GO sheets using methods like mild sonication.[30,31] Moreover, the abundant oxygen functionalities impart GO with a strong hydrophilic character, making it highly dispersible and stable in polar solvents like water.[32] GO suspensions can be easily cast into molds to fabricate freestanding GOFs through the gradual evaporation of water, typically achieved by annealing at a low temperature range of 50-60 °C. The abundant OCFGs in GO facilitate strong inter-sheet hydrogen bonding and van der Waals interactions, which contribute to the formation of cohesive, mechanically robust, and highly flexible GOF. The solution-casting method employed here allows precise control over the size and thickness of the resulting GOFs by adjusting key parameters such as the GO concentration, the volume of suspension cast, and the surface area of the mold.[14]

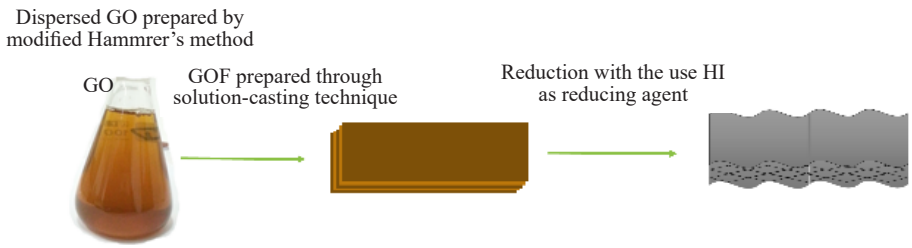

Figure 1. Schematic illustration of the fabrication process of RGOF

The reduction of GOFs was carried out chemically by treating the films with HI at a relatively low temperature of

60 °C. Unlike other reducing agents, HI possesses the unique advantage of preserving the freestanding structure and mechanical integrity of the GOF during reduction.[24] Regarding the underlying mechanism, studies have shown that HI initially facilitates the conversion of epoxy groups into hydroxyl groups. Subsequently, iodide ions (I^-) act as efficient nucleophiles, displacing the hydroxyl groups via substitution reactions. This stepwise reduction process leads to the effective removal of a significant portion of oxygen functionalities, thereby restoring the conjugated sp^2 carbon network and enhancing the electrical properties of the resulting RGOF.[33] Figure 1 illustrates the fabrication process of RGOFs from GO suspension.

When GO suspensions are reduced, the resulting RGO sheets tend to restack and agglomerate during drying. This is largely driven by strong van der Waals forces and π-π bonding between adjacent layers of graphene, causing the sheets to collapse into compact structures (Figure 2), thereby reducing accessible surface area and porosity.[34] In contrast, casting GO into a freestanding film before reduction effectively addresses this issue. As shown in Figure 2, the resulting film retains its structural integrity after deoxygenation, preserving the porous network formed through the removal of OCFGs.

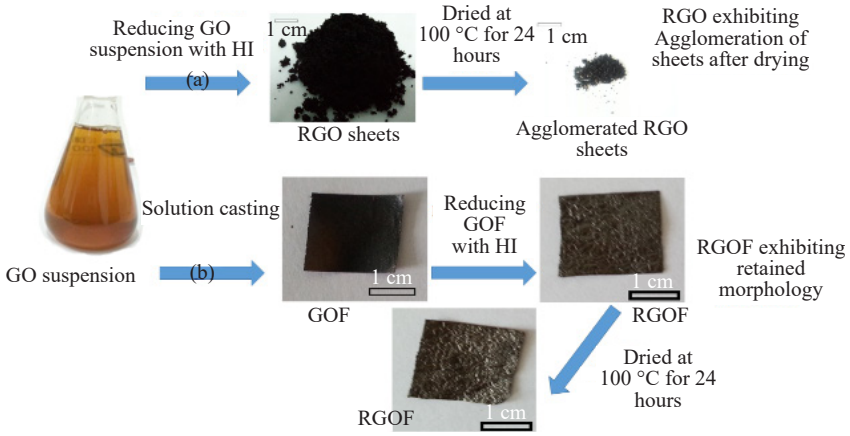

Figure 2. (a) Agglomeration observed in RGO sheets; (b) prevention of restacking and agglomeration through the formation of freestanding RGOF

3.2 *Electrical and mechanical characterization*

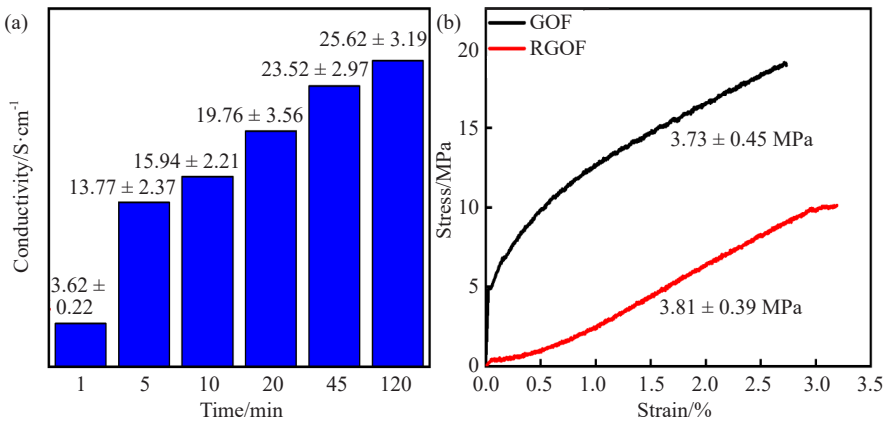

Figure 3. (a) Variation of the average electrical conductivity of GOF and RGOF as a function of reduction time. (b) Stress-strain curves of GOF and RGOF (130 μm thick)

The as-prepared RGOF demonstrates outstanding electrical conductivity, which improves progressively with

extended reduction time. As depicted in Figure 3a, the conductivity peaks at 2,564 $S \cdot m^{-1}$ after two hours of reduction, a result attributed to the efficient removal of OCFGs. This process restores the conjugated sp^2 carbon network, enabling more effective electron transport.[35] Significantly, the high conductivity of the RGOF allows it to serve directly as an electrode, eliminating the need for a separate current collector, thus streamlining the supercapacitor design and potentially lowering production costs.[36]

Beyond its electrical advantages, the RGOF also retains excellent mechanical flexibility. Following reduction, the film exhibits a modest 2% increase in elastic modulus and a notable gain in ductility. Although the elastic modulus of both GOF and RGOF is lower than values typically reported in the literature, this outcome stems from the solution casting method used in our GOF preparation.

3.3 *Morphological and spectral characterizations*

To gain insight into the morphology of the as-prepared graphene-based films, both the surface and cross-sectional structures of GOF were examined before and after chemical reduction. Notably, the surface morphology of the GOF remained largely unchanged following reduction with HI, exhibiting a smooth surface with slight wrinkling (Figure 4a and Figure 4b). This observation confirms that the use of HI as a chemical reducing agent preserves the structural integrity of the GOF without introducing significant surface damage.

In addition, cross-sectional SEM images (Figure 4c and Figure 4d) reveal substantial morphological changes induced by the reduction process. Prior to reduction, the GOF displayed a densely packed, layered structure. After reduction, however, the internal architecture transitioned into a more porous and loosely stacked configuration, characterized by increased interlayer spacing and the emergence of a fluffy, less compact morphology. This transformation can be attributed to the partial removal of OCFGs, which reduces van der Waals interactions and disrupts hydrogen bonding between adjacent layers. Additionally, the release of gaseous byproducts during the chemical reduction process contributes to the expansion of the film structure.

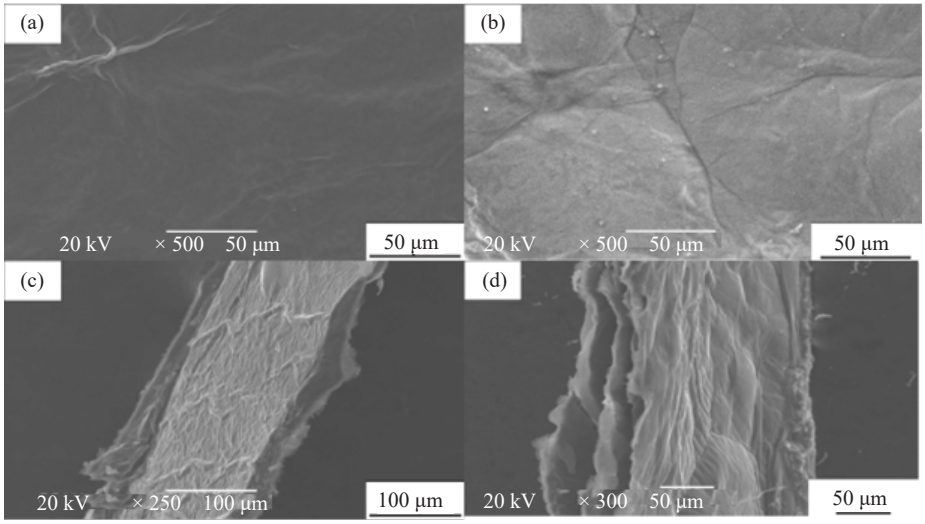

Figure 4. SEM images of (a) GOF and (b) RGOF surfaces. Cross-sectional SEM images of (c) GOF and (d) RGOF

The XRD patterns (Figure 5a) confirm the successful oxidation of natural graphite into GO. The XRD spectrum of GO shows a prominent peak at $2\theta \approx 10.1°$, indicating a significant increase in interlayer distance to around 8.8 Å. This expansion is attributed to the insertion of OCFGs and the formation of structural defects during the oxidation process. Upon the chemical reduction, GOF is converted into RGOF, accompanied by a shift of the diffraction peak to $2\theta \approx 24.4°$, corresponding to a decreased interlayer spacing of about 3.64 Å. This reduction in d-spacing suggests the partial removal of OCFGs and the partial restoration of the graphitic structure.

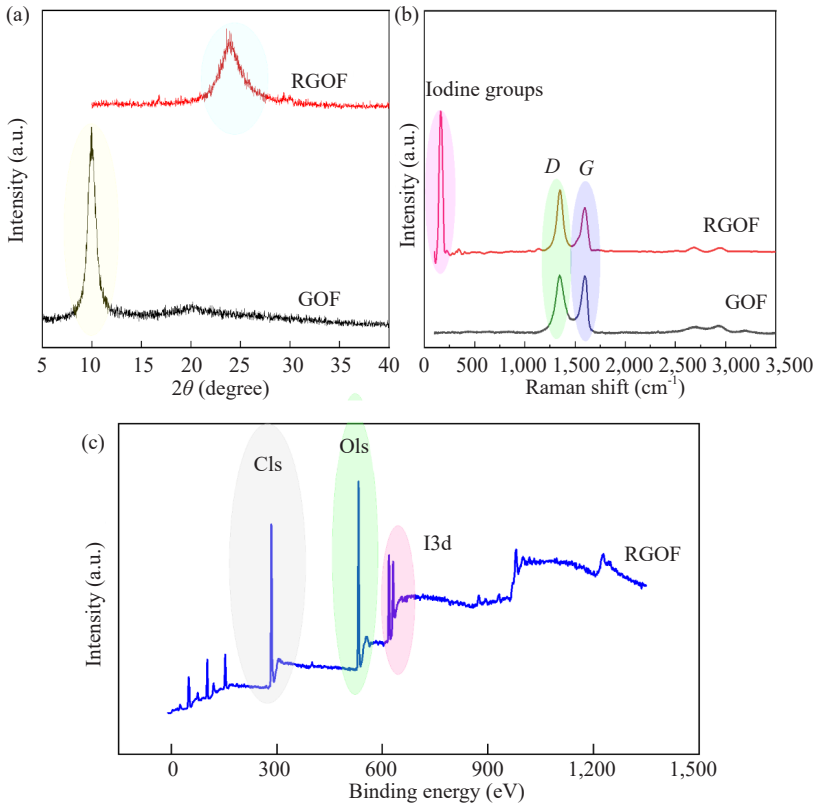

Figure 5. XRD patterns (a) and Raman spectroscopy (b) of GOF before and after 1 h reduction, (c) X-ray Photoelectron Spectroscopy (XPS) survey of RGOF

Raman spectroscopy, recognized for its non-destructive yet highly informative nature, was utilized to delve into the structural nuances of GBMs. As illustrated in Figure 5b, the Raman spectra of both GOF and RGOF highlight two major phonon bands: the *D* band (~ 1,340 cm^{-1}), which is tied to structural imperfections and the disorder brought on by OCFGs, and the *G* band (~ 1,590 cm^{-1}), reflecting the vibrational mode typical of sp^2 carbon atoms within the graphitic matrix. A crucial metric in evaluating graphene disorder is the intensity ratio between the *D* and *G* bands. For unmodified GOF, this ratio stands at roughly 0.93. However, following chemical reduction with HI, the ratio climbs to 1.41, pointing to a notable uptick in defect sites. This increase likely stems from both the removal of OCFGs and the integration of iodine atoms into the carbon framework. These structural disruptions arising from intrinsic defects such as vacancies and residual OCFGs, or deliberate modifications through heteroatom doping like iodine, play a pivotal role in enhancing the electrochemical performance of RGOFs. Such disruptions not only improve electrical conductivity by facilitating charge transport but also increase redox activity by introducing new active sites. Notably, the emergence of a distinct Raman peak around 160 cm^{-1} in the spectrum of RGOF serves as strong spectroscopic evidence for the successful incorporation of iodine atoms into the graphene lattice, indicating significant structural and chemical modification.[2,17] Moreover, the XPS survey confirms the successful incorporation of iodine functionalities, revealing that more than 6% iodine is present within the RGOF structure. In addition, approximately 26% oxygen is retained, indicating the presence of abundant OCFGs. These functional groups, particularly iodine and oxygen species, are expected to enhance the overall capacitance through their significant pseudocapacitive contribution.

3.4 *Electrochemical behavior*

The electrochemical performance of the as-prepared RGOF electrode was systematically evaluated using CV, GCD, and EIS. Prior to all measurements, the RGOF-based electrode was chemically treated with HI at 70 °C for 45 minutes.

Figure 6a and Figure 6b present CV curves and GCD profiles, respectively, of the RGOF-based electrode. The CV

curves display a quasi-rectangular shape superimposed with noticeable redox peaks, suggesting that the total capacitance originates from a combination of Electric Double-Layer Capacitance (EDLC) and pseudocapacitive contributions. The large specific surface area of the RGOF facilitates efficient ion adsorption at the electrode-electrolyte interface, thereby enhancing EDLC behavior. In parallel, the presence of residual OCFGs and introduced iodine species contributes to Faradaic redox reactions, which account for the observed pseudocapacitance.

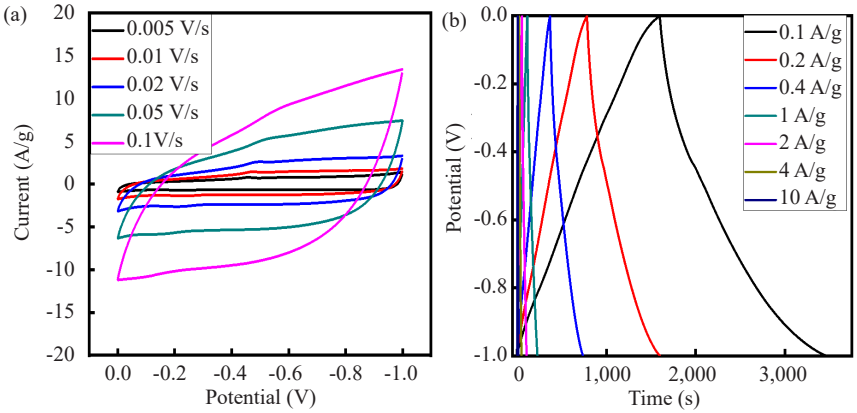

Figure 6. (a) CV curves of the RGOF-based electrode obtained at different scan rates; (b) GCD profiles of the RGOF-based electrode recorded at varying current densities

Moreover, GCD measurements were performed within the same potential window across a range of current densities. As illustrated, the charge-discharge curves exhibit a nearly symmetrical triangular shape with minimal Internal Resistance (IR) drop, even at a high current density of 10 $A \cdot g^{-1}$. This behavior indicates excellent electrochemical reversibility, rapid charge transport, and low internal resistance of the RGOF-based electrode. Additionally, the appearance of shoulder-like features and subtle deviations from ideal symmetry in the GCD curves further support the coexistence of EDLC and reversible Faradaic reactions, confirming a hybrid charge storage mechanism dominated by both EDLC and pseudocapacitance.

The specific capacitance ($C/F \cdot g^{-1}$) of the RGOF-based electrode was quantitatively determined from the discharge profiles of the GCD curves recorded at various current densities. The calculation was performed using the following standard equation:

$$C = i\frac{\Delta t}{m\Delta V} \tag{1}$$

where i (A) is the applied discharge current, Δt (s) is the discharge time, ΔV (V) is the potential window excluding the IR drop, and m (g) is the mass of the electroactive material deposited on the working electrode.

The calculated specific capacitance values are summarized in Table 1. The RGOF-based electrode demonstrates an impressive specific capacitance of 383 $F \cdot g^{-1}$ at a low current density of 0.4 $A \cdot g^{-1}$, highlighting its excellent charge storage capability under slow charging-discharging conditions. However, as the current density increases, the specific capacitance gradually declines, reaching 92 $F \cdot g^{-1}$ at 10 $A \cdot g^{-1}$.

This decrease is primarily attributed to kinetic limitations during high-rate charge-discharge processes. At elevated current densities, the time available for electrolyte ions to diffuse and access the internal pores of the electrode material becomes insufficient. As a result, only the outer surface or easily accessible active sites contribute to the capacitance, while deeper pores, especially those within agglomerated or densely stacked regions, remain underutilized. This diffusion-limited behavior is a common characteristic of graphene-based materials and reflects the trade-off between power and energy storage performance in supercapacitor systems.

Table 1. Specific capacitance of RGOF-based electrode at various current densities

Scan rates/A·g^{-1}	0.4	0.5	1	2	4	5	10
Capacity/F·g^{-1}	383.56	299.3	220.84	175.88	135.88	121.55	92.5

The long-term cycling stability of the RGOF-based electrode was evaluated by subjecting it to repeated CV measurements in the potential range of 0 to -1 V at a scan rate of 0.1 V·s^{-1} for 4,000 consecutive cycles, as shown in Figure 7. Remarkably, the electrode retained approximately 98% of its initial capacitance after 4,000 cycles, indicating excellent electrochemical durability. The stable cycling behavior suggests high reversibility of the charge storage mechanisms, including both EDLC and pseudocapacitance, without significant degradation of active material.

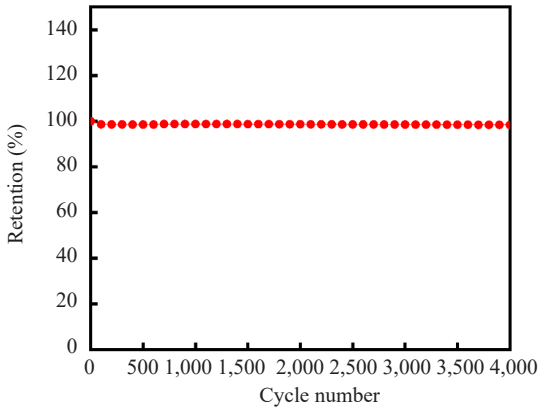

Figure 7. Cycling performance of the RGOF-based electrode evaluated over 4,000 consecutive CV cycles at a scan rate of 0.1 V·s^{-1} within a potential window of 0 to -1 V

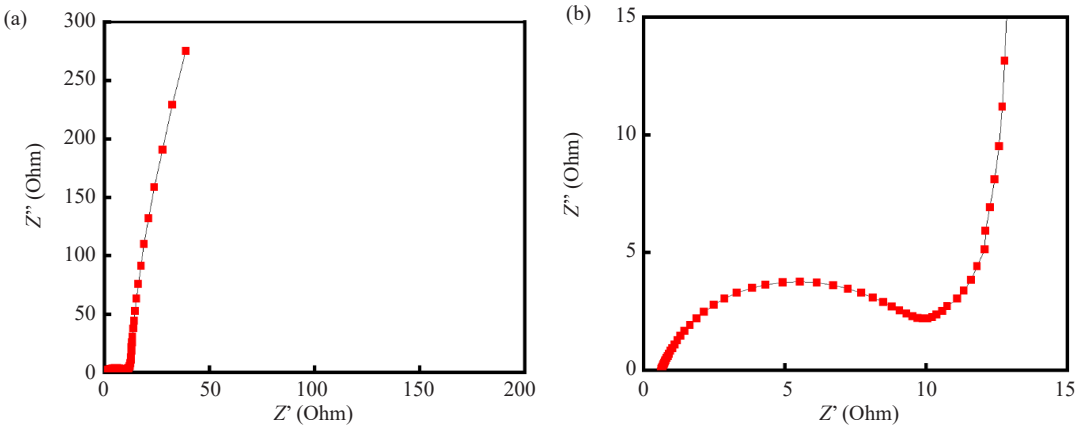

Figure 8. (a) Nyquist plot of the RGOF-based electrode recorded in the frequency range of 100 kHz to 0.005 Hz; (b) magnified view of the high-frequency region

EIS is a well-established technique for probing the interfacial charge transport and electrochemical kinetics of electrode materials, particularly in supercapacitor applications.[37] Figure 8 presents the Nyquist plot of the as-prepared RGOF-based electrode, offering valuable insights into its resistive and capacitive behavior. The plot features two distinct regions: a small semicircle in the high-frequency domain and a nearly vertical line in the low-frequency region. The small semicircle represents the combined effects of charge transfer resistance (R_{ct}) at the electrode-electrolyte interface

and intrinsic electronic resistance within the electrode material. The relatively small diameter of this arc indicates low internal resistance and efficient charge transfer processes.

Meanwhile, the steep, almost vertical line at low frequencies is characteristic of ideal capacitive behavior, reflecting dominant electric double-layer formation and effective ion diffusion within the porous RGOF structure. The high slope suggests minimal diffusion limitations and a capacitive response approaching that of an ideal supercapacitor. The negligible arc size and pronounced verticality of the low-frequency tail together confirm the excellent electrical conductivity and efficient ion/electron transport pathways in the RGOF, likely due to the well-stacked yet highly accessible graphene network.[38]

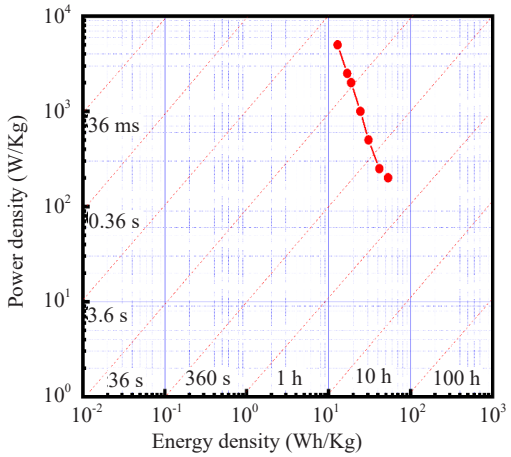

Figure 9. Ragone plot illustrating the relationship between energy density and power density for the RGOF-based electrode

The Ragone plot (Figure 9) illustrates the trade-off between energy density and power density for the RGOF-based electrode, providing a comprehensive assessment of its electrochemical performance. The maximum energy density was calculated using the following equation:

$$E = \frac{1}{2} C \Delta V^2 \tag{2}$$

Where E is the energy density ($Wh \cdot kg^{-1}$), C is the specific capacitance ($F \cdot g^{-1}$), and ΔV is the voltage window, taken as 1 V in this study. The corresponding power density was derived using:

$$P = \frac{E}{t} \tag{3}$$

Where P is the power density ($W \cdot kg^{-1}$), and t is the discharge time (s) obtained from the GCD measurements.

These two metrics, energy and power densities, highlight the ability of the RGOF-based electrode to deliver both high energy storage and rapid charge/discharge capability. As observed in the Ragone plot, the as-obtained RGOF-based electrode exhibits a high energy density of 53.3 $Wh \cdot kg^{-1}$ at a power density of 200 $W \cdot kg^{-1}$, which can be attributed to its high specific capacitance.

The relatively high energy density of the RGOF-based electrode can be attributed to the synergistic contributions of multiple charge-storage mechanisms. First, pseudocapacitance (faradaic capacitance) arises from residual OCFGs and the incorporation of iodine atoms, both of which provide additional redox-active sites. Second, the EDLC is enhanced by the enlarged specific surface area generated during the reduction process. The introduction of iodine not only creates localized defects and heteroatom sites that supply extra pseudocapacitive centers but also improves electrolyte wettability, further promoting capacitive behavior. In addition, the freestanding structure of the RGOF, combined

with the mild HI reduction that avoids structural damage, preserves excellent electrical conductivity. This high conductivity ensures efficient ion transport and uniform electrolyte penetration throughout the interconnected network of electrochemically active sites, thereby maximizing the overall energy storage performance.

Looking ahead, improving the rate capability of RGOFs at high current densities may be achieved through pore engineering strategies that optimize ion diffusion pathways, as well as doping optimization to tailor surface functionalities for faster redox kinetics. Moreover, exploring the use of alternative electrolytes, such as ionic liquids or organic-based systems, could significantly extend the operating voltage window beyond aqueous limits, thereby boosting energy density and enhancing compatibility with practical device applications.

4. Comparative analysis

The data presented in Table 2 summarizes recently reported electrode materials for supercapacitors in terms of preparation method, specific capacitance, energy density, and long-term cycling stability. Combining RGO with various functional materials, such as MXenes, conducting polymers, and metal oxides, has led to the development of highly effective active materials for supercapacitors. For instance, RGO/MXene-PPy composites prepared via solvent-assisted assembly deliver a high capacitance of 408 $F \cdot g^{-1}$ with good retention.[39] While CNT-Fe_3O_4/RGO composites fabricated by electrophoresis exhibit relatively higher energy density and stable cycling.[40] Furthermore, multi-step treatments can effectively enhance the supercapacitive performance of RGOFs; for example, RGOFs obtained through two-step thermochemical reduction achieve a balanced combination of capacitance and stability.[2] In addition, other carbon-based materials also show promise, as biomass-derived activated carbon electrodes demonstrate excellent cycling durability with moderate capacitance values.[41] Notably, our flexible RGOFs, produced via a simple one-pot chemical reduction using HI as the reducing agent, exhibit a favorable combination of high capacitance, enhanced energy density, and stable cycling behavior, confirming their suitability as efficient electrodes for flexible supercapacitor applications.

Table 2. Comparative electrochemical performance of supercapacitor materials from recent literature

Material System	Preparation method	Specific capacitance	Energy density	Cycling stability
RGO/MXene-PPy composite film[39]	Solvent-assisted assembly	408 $F \cdot g^{-1}$ (1 $A \cdot g^{-1}$)	11.3 $W \cdot h \cdot kg^{-1}$	8.8% loss after 10,000 cycles
CNT-Fe_3O_4/RGO flexible composite[40]	Electrophoresis	275.6 $F \cdot g^{-1}$ (1 $A \cdot g^{-1}$)	36.7 $W \cdot h \cdot kg^{-1}$	~ 92.9% retention after 10,000 cycles
Flexible RGOF[2]	Thermochemical reduction	350.44 $F \cdot g^{-1}$ (0.5 $A \cdot g^{-1}$)	12.82 $W \cdot h \cdot kg^{-1}$	93% retention (7% loss) after 5,000 cycles
Cotton-shell-derived activated carbon[41]	Heat treatment	247.8 $F \cdot g^{-1}$ (0.52 $A \cdot g^{-1}$)	22.6 $W \cdot h \cdot kg^{-1}$	97% retention (3% loss) after 10,000 cycles
Flexible RGOF (Our study)	Chemical treatment with HI	383 $F \cdot g^{-1}$ (0.4 $A \cdot g^{-1}$)	53 $W \cdot h \cdot kg^{-1}$	98% retention (2% loss) after 4,000 cycles

5. Conclusion

This study presents a one-pot, cost-effective chemical reduction method for synthesizing RGOFs using hydroiodic acid. The resulting RGOFs exhibit notable flexibility and high electrical conductivity, as confirmed by electrical and mechanical assessments. Structural analyses through XRD and Raman spectroscopy validate the successful reduction of GOF with the incorporation of iodine groups into its structure. Electrochemical investigations reveal that the RGOFs deliver an exceptional specific capacitance of 380 $F \cdot g^{-1}$ and operate efficiently within a voltage window of 1 V in an aqueous solution. Notably, they achieve an impressive energy density of around 53 $Wh \cdot kg^{-1}$. The simplicity of the fabrication process, combined with the scalability and low cost of graphene production, positions these RGOFs as excellent candidates for next-generation, low-cost, ultrahigh-energy storage solutions in PFEDs. Future feasibility studies should investigate the integration of RGOFs into flexible device prototypes and evaluate their performance with alternative electrolytes.

Acknowledgment

The authors extend their heartfelt thanks to all those who have supported and contributed to this work, whether through technical assistance, insightful discussions, or moral support.

Conflict of interest

Authors declare that they have no known competing financial interests or personal relationships that could have appeared to influence the work reported in this paper.

References

[1] Shi, X.; Tian, L.; Wang, S.; Wen, P.; Su, M.; Xiao, H.; Das, P.; Zhou, F.; Liu, Z.; Sun, C.; et al. Scalable and fast fabrication of graphene integrated micro-supercapacitors with remarkable volumetric capacitance and flexibility through continuous centrifugal coating. *J. Energy Chem.* **2020,** *52*, 284-290.
[2] Akbi, H.; Rafai, S.; Mekki, A.; Touidjine, S.; Belkadi, K.; Boudina, N.; Rabah, I. Boosting the storage capacity and the rate capability of flexible graphene film via a nondestructive thermo-chemical reduction. *Diam. Relat. Mater.* **2022,** *129*, 109338.
[3] Winter, M.; Brodd, R. J. What are batteries, fuel cells, and supercapacitors. *Chem. Rev.* **2004,** *104*(10), 4245-4269.
[4] Wang, G.; Zhang, L.; Zhang, J. A review of electrode materials for electrochemical supercapacitors. *Chem. Soc. Rev.* **2012,** *41*(2), 797-828.
[5] Yan, J.; Wang, Q.; Wei, T.; Fan, Z. Recent advances in design and fabrication of electrochemical supercapacitors with high energy densities. *Adv. Energy Mater.* **2014,** *4*(4), 1300816.
[6] Conway, B. E. *Electrochemical Supercapacitors*; Springer US: Boston, MA, 1999.
[7] Horn, M.; Gupta, B.; MacLeod, J.; Liu, J.; Motta, N. Graphene-based supercapacitor electrodes: addressing challenges in mechanisms and materials. *Curr. Opin. Green Sustain. Chem.* **2019,** *17*, 42-48.
[8] Xiong, C.; Li, B.; Lin, X.; Liu, H.; Xu, Y.; Mao, J.; Duan, C.; Li, T.; Ni, Y. The recent progress on three-dimensional porous graphene-based hybrid structure for supercapacitor. *Compos. B Eng.* **2019,** *165*(2), 10-46.
[9] Thomas, R.; Manoj, B. Fabrication approaches for graphene in supercapacitors. *Mater. Res. Found.* **2020,** *64*, 1-24.
[10] Capaz, R. B. Grand challenges in graphene and graphite research. *Front. Carbon* **2022,** *1*, 1034557.
[11] Akbi, H.; Mekki, A.; Rafai, S.; Boulkadid, M. K.; Touidjine, S.; Belgacemi, R.; Chabane, H.; Bekkar Djeloul Sayeh, Z. Preventing agglomeration and enhancing the energetic performance of fine ammonium perchlorate through surface modification with hydrophobic reduced graphene oxide. *ChemistrySelect* **2024,** *9*(1), e202301795.
[12] Mypati, S.; Sellathurai, A.; Kontopoulou, M.; Docoslis, A.; Barz, D. P. J. High concentration graphene nanoplatelet dispersions in water stabilized by graphene oxide. *Carbon* **2021,** *174*, 581-593.
[13] Akbi, H.; Rafai, S.; Mekki, A.; Touidjine, S.; Fertassi, M. A.; Kadri, D. E. When copper oxide meets graphene oxide: a core-shell structure via an intermittent spray coating route for a highly efficient ammonium perchlorate thermal decomposition. *J. Organomet. Chem.* **2022,** *957*, 122159.
[14] Akbi, H.; Mekki, A.; Rafai, S.; Touidjine, S.; Boudina, N.; Bekkar Djeloul Sayeh, Z. Phenomenological description of the thermal reduction kinetics in graphene oxide films. *Mater. Chem. Phys.* **2022,** *277*, 125477.
[15] Akbi, H.; Rafai, S.; Mekki, A.; Bekhouche, S.; Touidjine, S.; Louafi, E.; Saim, A.; Hamouche, M. A. Model-free kinetic analysis of multi-step thermal decomposition of ammonium perchlorate coated with reduced graphene oxide. *Reaction Kinetics, Mechanisms and Catalysis* **2025,** *138*(1), 125-142.
[16] Akbi, H.; Yu, L.; Wang, B.; Liu, Q.; Wang, J.; Liu, J.; Song, D.; Sun, Y.; Liu, L. Effect of reducing system on capacitive behavior of reduced graphene oxide film: application for supercapacitor. *J. Solid State Chem.* **2015,** *221*, 338-344.
[17] Akbi, H.; Rafai, S.; Riou, O.; Mekki, A.; Durastani, J.-F.; Bekkar Djeloul Sayeh, Z.; Touidjine, S. Flexible and lightweight thermoelectric generator based on chemically and thermally prepared reduced graphene oxide films. *Mater. Chem. Phys.* **2025,** *344*, 131071.

[18] Han, H. J.; Chen, Y. N.; Wang, Z. J. Effect of microwave irradiation on reduction of graphene oxide films. *RSC Adv.* **2015,** *5*(113), 92940-92946.
[19] Akbi, H.; Rafai, S.; Mekki, A.; Touidjine, S.; Hamouche, M. A. Correlating heat treatment conditions with the physicochemical properties of thermally reduced graphene oxide-based materials: a comprehensive review. *Universal J. Carbon Res.* **2024,** *2*(2), 1-43.
[20] You, R.; Liu, Y. Q.; Hao, Y. L.; Han, D. D.; Zhang, Y. L.; You, Z. Laser fabrication of graphene-based flexible electronics. *Adv. Mater.* **2019,** *32*(15), 1901981.
[21] Ai, X.; Zhang, P.; Dou, Y.; Wu, Y.; Pan, T.; Chu, C.; Cui, P.; Ran, J. Graphene oxide membranes with hierarchical structures used for molecule sieving. *Sep. Purif. Technol.* **2020,** *230*, 115879.
[22] Cao, J.; Chen, C.; Zhao, Q.; Zhang, N.; Lu, Q.; Wang, X.; Niu, Z.; Chen, J. A flexible nanostructured paper of a reduced graphene oxide-sulfur composite for high-performance lithium-sulfur batteries with unconventional configurations. *Adv. Mater.* **2016,** *28*(43), 9629-9636.
[23] Akbi, H.; Rafai, S.; Mekki, A. Reduced graphene oxide film with an ultrahigh energy density for batterylike supercapacitor. In *Materials Chemistry: Proceedings Book of the 2nd International Symposium*; Irekti, A., Ed.; International Symposium on Materials Chemistry, 2021; pp 21.
[24] Pei, S.; Zhao, J.; Du, J.; Ren, W.; Cheng, H. M. Direct reduction of graphene oxide films into highly conductive and flexible graphene films by hydrohalic acids. *Carbon* **2010,** *48*(15), 4466-4474.
[25] Kamila, S.; Kandasamy, M.; Chakraborty, B.; Jena, B. K. The role of iodine in the enhancement of the supercapacitance properties of HI-treated flexible reduced graphene oxide film: an experimental study with insights from DFT simulations. *New J. Chem.* **2020,** *44*(4), 1418-1425.
[26] Hummers, W. S.; Offeman, R. E. Preparation of graphitic oxide. *J. Am. Chem. Soc.* **1958,** *80*(6), 1339-1339.
[27] Akbi, H.; Rafai, S.; Mekki, A.; Touidjine, S.; Belkadi, K. Kinetic investigation of the multi-step thermal decomposition of graphene oxide paper. *J. Therm. Anal. Calorim.* **2023,** *148*(9), 3487-3503.
[28] Novais Antunes, F. P.; Vaiss, V. S.; Tavares, S. R.; Capaz, R. B.; Leitão, A. A. Van der Waals interactions and the properties of graphite and 2H-, 3R- and 1T-MoS2: a comparative study. *Comput. Mater. Sci.* **2018,** *152*, 146-150.
[29] Shao, G.; Lu, Y.; Wu, F.; Yang, C.; Zeng, F.; Wu, Q. Graphene oxide: the mechanisms of oxidation and exfoliation. *J. Mater. Sci.* **2012,** *47*, 4400-4409.
[30] Foong, H. L.; Tan, C. P.; Mohd Zawawi, R.; Z. A., N. H. Effect of sonication time and heat treatment on the structural and physical properties of chitosan/graphene oxide nanocomposite films. *Food Packag. Shelf Life* **2021,** *28*(2), 100663.
[31] Choucair, M.; Thordarson, P.; Stride, J. A. Gram-scale production of graphene based on solvothermal synthesis and sonication. *Nat. Nanotechnol.* **2009,** *4*(1), 30-33.
[32] Paredes, J. I.; Villar-Rodil, S.; Martínez-Alonso, A.; Tascón, J. M. D. Graphene oxide dispersions in organic solvents. *Langmuir* **2008,** *24*(19), 10560-10564.
[33] Moon, I. K.; Lee, J.; Ruoff, R. S.; Lee, H. Reduced graphene oxide by chemical graphitization. *Nat. Commun.* **2010,** *1*, 73.
[34] Li, J.; Östling, M. Prevention of graphene restacking for performance boost of supercapacitors-a review. *Crystals* **2013,** *3*(1), 163-190.
[35] Mattevi, C.; Eda, G.; Agnoli, S.; Miller, S.; Mkhoyan, K. A.; Celik, O.; Mastrogiovanni, D.; Granozzi, G.; Carfunkel, E.; Chhowalla, M. Evolution of electrical, chemical, and structural properties of transparent and conducting chemically derived graphene thin films. *Adv. Funct. Mater.* **2009,** *19*(16), 2577-2583.
[36] El-Kady, M. F.; Strong, V.; Dubin, S.; Kaner, R. B. Laser scribing of high-performance and flexible graphene-based electrochemical capacitors. *Science* **2012,** *335*(6074), 1326-1330.
[37] Navalpotro, P.; Anderson, M.; Marcilla, R.; Palma, J. Insights into the energy storage mechanism of hybrid supercapacitors with redox electrolytes by electrochemical impedance spectroscopy. *Electrochim. Acta* **2018,** *263*, 110-117.
[38] Wang, Y.; Shi, Z.; Huang, Y.; Ma, Y.; Wang, C.; Chen, M.; Chen, Y. Supercapacitor devices based on graphene materials. *J. Phys. Chem. C* **2009,** *113*(30), 13103-13107.
[39] Wang, G.; Jiang, N.; Xu, Y.; Zhang, Z.; Wang, G.; Cheng, K. Solvent-assisted assembly of reduced graphene oxide/MXene-polypyrrole composite film for flexible supercapacitors. *J. Colloid Interface Sci.* **2023,** *630*, 817-827.
[40] Xie, S.; Dong, F.; Li, J. Flexible solidstate supercapacitor based on carbon nanotube/Fe_3O_4/reduced graphene oxide binary films. *ChemSelect* **2019,** *4*(1), 437-440.
[41] Singh, S.; Zhang, Y.; Hashmi, S. A.; Yang, F. Supercapacitors with cotton shell-derived activated carbons and porous polymer electrolyte films. *RSC Adv.* **2025,** *15*(13), 9787-9800.